Journal of Nanoscience and Nanotechnology
Vol. 10, 6348–6355, 2010

Magnetic Fe_3O_4@Chitosan Nanoparticle: Synthesis, Characterization and Application as Catalyst Carrier

Linghao He[1], Lu Yao[1], Fujun Liu[1], Bing Qin[2], Rui Song[1,2,*], and Wei Huang[3,*]

[1] *Key Lab of Surface and Interface Sciences of Henan Provincial, Zhengzhou University of Light Industry, Zhengzhou, China 450005*
[2] *College of Chemistry and Chemical Engineering, Graduate University of Chinese Academy of Sciences, Beijing, China 100049*
[3] *Laboratory of Materials of High Technology, Institute of Chemistry, Chinese Academy of Sciences, Beijing, China 100080*

A novel method was developed to prepare Fe_3O_4@CS beads with core–shell structure using a *double-crosslinking* process. Before the coating process, an unique crosslinking agent, glutaraldehyde (GA), was adsorbed onto the surface of Fe_3O_4 in advance, so the subsequent CS can uniformly coat around the magnetic core processed from the strong interaction between GA and CS, forming a perfect core–shell structure. The obtained Fe_3O_4@CS beads were followed by the Pd deposition through *in-situ* reduction method, and the prepared composite catalyst was applied exemplarily in synthesizing nabumetone to check its reusing property. The nanoparticles were characterized by transmission electron microscopy (TEM), X-ray powder diffraction (XRD), Fourier transformation infrared spectroscopy (FTIR), X-ray photoelectron spectroscopy (XPS), and the magnetic hysteresis loop determination method. This novel composite catalyst showed admirable potential in reusable catalysis.

Keywords: Superparamagnetic Nanoparticles, Double-Crosslinking, Core–Shell Structure, Pd Deposition, Reusable Catalyst.

1. INTRODUCTION

Superparamagnetic nanoparticles are attracting increasing attentions for their advanced properties and wide applications such as magnetic resonance imaging (MRI) contrast enhancement,[2] tissue repair,[3] immunoassay,[4] detoxification of biological fluids,[5] hyperthermia,[6] drug delivery[7] and cell separation,[8] etc. In the last decade, several types of iron oxides have been successively carried out in the field of superparamagnetic nanoparticles (mostly maghemite or magnetite, with the diameter of about 5–20 nm), among which the magnetite, Fe_3O_4, is a very promising candidate for its outstanding biocompatibility. Magnetite, Fe_3O_4, is a common paramagnetic iron oxide that has a cubic inverse spinel structure, where oxygen forms an fcc closed packing and Fe cations occupy the interstitial tetrahedral sites and octahedral sites, with a stoichiometric ratio of 2:1 (Fe^{3+}/Fe^{2+}) in a non-oxidizing oxygen environment.[9] As an important half-metallic material, the electrons of magnetite can hop between Fe^{3+} and Fe^{2+} irons at room temperature. So various synthetic methods have been reported for the preparation of nanoscale Fe_3O_4 particles, including the reduction of hematite Fe_2O_3 by H_2 or CO,[10] coprecipitation of an aqueous solution of ferrous and ferric ions by a base,[11] oxidation of the ferrous hydroxide gels using KNO_3 or $(NH_4)_2S_2O_8$,[12] γ-ray irradiation,[13] microwave plasma synthesis,[14] polyol-mediated sol–gel,[15] sonochemistry,[16] oil-in-water emulsion route using a small amount of cyclohexane as the oil phase,[17] hydrothermal reaction,[18] nonaqueous route,[19] etc. However, the method of chemical coprecipitation, in the view of economy and environmental benignancy, will be the most ideal among the above methods because water which is nontoxic is used as the reaction medium and it doesn't require too much heat to maintain a high temperature as in the case of hydrothermal reaction.

In spite of its outstanding biocompatibility, Fe_3O_4 nanoparticles cannot be directly used in the practical applications with its uncovered surface exposed to the wild environment, owing to the high surface energy for its large ratio of surface area to volume.[20] In oxidizing environment magnetite is not very stable and is readily to be oxidized into maghemite (γ-Fe_2O_3). Not only nonresistant to the oxygen, magnetite is also not stable in acidic and anaerobic medium, which is always applied for biomedical applications, since various electron or ion transfers will occur depending upon the pH of the suspension, which involves an oxidation–reduction reaction of the surface of magnetite.[21] The oxidation–reduction process

---

[*] Authors to whom correspondence should be addressed.

1533-4880/2010/10/6348/008 doi:10.1166/jnn.2010.2549

of ferrous ions is mainly made up of the migration of cations through the lattice framework and the forming of cationic vacancies to keep the charge, forming the structure of maghemit. In maghemite, iron ions are distributed in the octahedral (Oh) and tetrahedral (Td) sites of the spinel structure ($0.75[Fe^{3+}]_{Td}[Fe^{3+}_{5/3}V_{1/3}]_{Oh}O_4$), which differs from magnetite ($[Fe^{3+}]_{Td}[Fe^{3+}Fe^{2+}]_{Oh}O_4$) by the presence of cationic vacancies within the octahedral site. The vacancies ordering scheme is closely related to the sample preparation method and results in lowering symmetry and possibly superstructures. The vacancies can be completely random or partially or totally ordered.

To overcome the instability of magnetite, the surfaces of these particles must be modified through the creation of few atomic layers of organic polymer or inorganic metallic (e.g., gold) or oxide surfaces (e.g., silica or aluminum), suitable for further function by the attachment of various bioactive molecules.[22] One the other hand, the coating of suitable layer can also prevent the aggregation of magnetite nanoparticles caused mainly by van der Waals forces and magnetic dipolar forces, which specially exist only for magnetic particles. For magnetic suspensions, magnetic dipolar forces between two particles introduce anisotropic interactions, which will be very important when if the anisotropic interparticle potential is integrated over all directions. The adding of the coating layer, accomplished by physical or chemical adsorption, has been proved to be effective in the prevention of the unexpected aggregation and improving the chemical stability of composite system.

Chitosan (noted as CS), a cationic linear polysaccharide composed essentially of $\beta(1\rightarrow4)$ linked glucosamine units together with some proportion of N-acetylglucosamine units, is of interest as a potential coating component because of its excellent biocompatibility and biodegradation property.[23] Generally obtained from natural chitin after deacetylation by alkaline treatments, CS is a natural, nontoxic and biodegradable polymer that is commercially available and can be produced from shellfish waste.[24] Recently materials scientists started to be interested in the utilization of CS as a coating material to synthesize composites. Ding et al. synthesized Fe_3O_4/CS-PAA hollow spheres using glutaraldehyde (GA) as crosslinking agent.[25] From the TEM results, the as-obtained hybrid hollow spheres presented an anomalous shape which was different from uncovered Fe_3O_4 nanoparticles with an integrate sphere shape. The reason of the discrepancy between shapes of Fe_3O_4/CS-PAA and Fe_3O_4 would be the asymmetric loading of CS in the surface of Fe_3O_4. The asymmetric loading will lead to the incomplete coating and the partly bareness of Fe_3O_4, so the faces with high surface energy will be exposed to wild environment, which will weaken the effect of coating.

In this case, we described a novel method, called 'double-crosslinking' to synthesize Fe_3O_4@CS hybrid beads with regularly spherical shape. GA was adopted as crosslinking agent to be absorbed onto the surface of Fe_3O_4 before CS loading, to make sure CS can be uniformly deposited on the surrounding of Fe_3O_4. After CS loading, GA was used again to crosslink the adsorbed CS, so that the solvent resistance of as-obtained nanosphere would be enhanced. A schematic drawing of the coating process is given in Scheme 1 to show how CS can be adsorbed to form the core–shell structure with this double crosslinking method. To study the potential of the obtained Fe_3O_4@CS as one catalyst carrier, palladium was deposited, by a *in-situ* reduction method on the surface of magnetic beads, to prepare composite catalyst Fe_3O_4@CS/Pd. The role of this catalyst was signified in the following synthesizing of nabumetone to investigate the catalytic efficiency. And the experimental data shown the catalyst had a high catalytic efficiency as the yield can reach more than 90; in addition, its recycle property was checked.

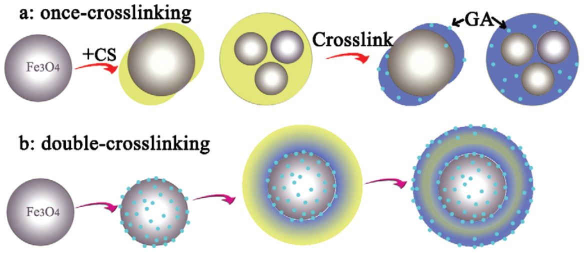

Scheme 1. Schematic drawing of the coating process of Fe_3O_4@CS nanoparticles, (a) with conventional once-crosslinking; (b) with novel double-crosslinking. The yellow surroundings denote the original CS without crosslinking, while the blue ones denote CS crosslinked by GA.

2. EXPERIMENTAL DETAILS

2.1. Materials

All the chemicals were of reagent grade and purified before used. Deionized water was re-deionized (electrical resistivity $\geq$18.2 M$\Omega \cdot$cm, 25 °C) and deoxygenated by boiling for 1 h before used. Ferric sulphate ($Fe_2(SO_4)_3$), ferrous sulphate heptahydrate ($FeSO_4 \cdot 7H_2O$, >99%) were obtained from Kemel chemical reagent Co. Ltd., Tianjin, China. Chitosan (deacetylation degree $\geq$92%, M_n = 79 500 g mol^{-1}, M_w = 88 700 g mol^{-1}, PDI = 1.12, as determined by GPC measurements) used for the particle coating process was purchased from Huoshuo fine chemical Co. Ltd., Shanghai, China. Glutaraldehyde (GA) 50% water solution was purchased from Kemel chemical reagent Co. Ltd., Tianjin, China. Palladium chloride ($PdCl_2$ > 99%), 2-bromo-6-methoxynaphthalene ($C_{11}H_9BrO$, 98%) and 3-buten-2-ol (C_4H_8O, 70%) were purchased from Alfa Aesar.

2.2. Synthesis of Magnetite

Fe_3O_4 was prepared without any additional stabilizer according to a controlled coprecipitation approach that could be found elsewhere.[11] In a typical synthesis, an aqueous mixture of ferric and ferrous solution (20.6 g) was dropped into and alkalinized by 10% NaOH solution (75 ml) at room temperature under mechanical stirring (500 rpm) in a three necked flask. N_2 gas was inflated during synthesis in a closed system to prevent the oxidization of Fe^{2+}. When a light black sedimentation appeared, the crystal growth was allowed to proceed for 1 hour with constant stirring to produce a stable, water-based suspension. The expectant products were isolated from the solvent by an external magnetic field followed by redispersed in deionized water. This washing-redispersion procedure was repeated several times until this colloid system was neutrality.

2.3. Coating of Magnetite by CS

As the as-prepared Fe_3O_4 nanoparticles (500 mg) were completely washed and redispersed into a transparent suspension, several drops of aqueous solution of GA, ca. 100 μL were dropped to the reaction system with continual stirring of 500 rpm for 1 hour to form a adsorption layer round Fe_3O_4. Then the above procedures of washing and redispersion were adopted again to remove the no-adsorbed GA. After the redispersion procedure, a CS solution (1% w/v) prepared by dissolving of 0.2 g of CS in 20 mg acetic acid was added to the reaction system followed by the coating process for 2 hours. To crosslink the exterior of loaded CS layer, GA was dropped into the flask again. 2 h later, the crosslinking reaction was completed and the final products was gathered with a permanence magnet and dried in an oven at 50 °C under vacuum for 24 hours.

2.4. Deposition of Palladium and Evaluation of Catalytic Properties

To prepare Fe_3O_4@CS/Pd, the obtained Fe_3O_4@CS disperse system (ca. 1.176 g) was mixed with $PdCl_2$ solution (0.52% w/v) by stirring overnight under N_2 atmosphere to absorb Pd^{2+} ion to the amino of CS out of co-ordination. Then the mixture was heated under reflux at 140 °C for 4 h, which process was also under N_2 gas inflating. After separated from the solution by a magnet, the orange production was dispersed in deionized water with another portion of $PdCl_2$ solution, followed by the reflux operation. Then the above process was repeated times to obtain the most palladium deposition.

The catalytic effect of the obtained composite catalyst was determined via the synthetic experiment of nabumetone, an important drug intermediate. The composite catalyst, approximately 210 mg was dispersed in 100 mL ethanol with 2-bromo-6-methoxynaphthalene (6.7 g) and 3-buten-2-ol (4.4 g), refluxed at 140 °C for 24 h. Then the magnetic catalyst was separated by a magnet, and the remaining solution was treated through distillation, to obtain the crystalline powder.

2.5. Characterization

X-ray powder diffraction (XRD) measurement was performed using a Bruker D8 diffractometer with monochromatized Cu Kα radiation ($\lambda = 1.5418$ Å), 40 kV, 30 mA. A continuous scan mode was used to collect 2-theta data from 10 to 90° with a 0.04 sample pitch and a 4° min^{-1} scan rate. Fourier transform infrared spectroscopy (FT-IR, Tensor 27, Bruker Inc.) was used to conform the chemical abstraction between the starch layer and the surface of magnetite particles. A JEM 200 CX transmission electron microscope (TEM) equipped with a CCD was used for high-resolution images of suspension samples, operated at an accelerating voltage of 200 kV. The specimen for TEM imaging was prepared from the Fe_3O_4@CS suspension in deionized water under sonication for 5 min. After sonication, a drop of well-dispersed suspension was placed on a carbon-coated copper grid, followed by drying at an oxygen-free environment before it was laid on the sample holder of the microscope. X-ray photoelectron spectroscopy (XPS) was performed using a VG Scientific ESCALab220i-XL photoelectron spectrometer equipped with a twin anode, providing both unchromatized AlKα radiations (1486.6 eV). The spectrometer, which was equipped with a multichannel detector, operated at 300 W and the C1s (284.8 eV) was choose as the reference line. Magnetic measurements were done in a vibrating sample magnetometer (VSM, PPMS-9, Quantum Design). The sample powder was placed in a Teflon-coated sample holder and the mass was accurately measured. The mass magnetization, M (Am^2kg^{-1}), was measured for different applied magnetic fields, at 300 K.

3. RESULTS AND DISCUSSION

3.1. Synthesis of Fe_3O_4@CS

Preparation of the crystal particles in the corresponding solution under optimum reaction conditions can be divided into two stages: the formation of tiny crystalline nuclei occurs when the concentration of the species reaches critical supersaturation, i.e., nucleation, and then the growth of the nuclei by diffusion of the solutes to the surface of the crystal. Here, among all of the particles with slightly different sizes, the large particles will grow larger at the cost of that with small size. This crystallization mechanism is called Ostwald ripening and has been generally accepted to be the main path of the crystal growth.[26]

As the comparison given in the scheme of synthesizing Fe_3O_4@CS nanoparticles in Scheme 1, CS is directly absorbed to the surface of Fe_3O_4 particles by electrostatic force and then crosslinked by subsequently added crosslinking agent, which will lead to the incomplete coating and some aggregate (showed in Scheme 1(a)). To get ideal core–shell structure, the crosslinking agent was added into the synthesis system in advance, so a layer of crosslinking agent will be uniformly absorbed to the surface of magnetic core, to induce a strong electrostatic force between the iron oxide nanoparticles and the organic crosslinking agent (as in Scheme 1(b)). Thus, via the double-crosslinking, the biocompatible CS can form a robust coating layer around the surface of magnetic core, which leads to a perfect core–shell structure.

As visually manifested in the TEM pictures (Fig. 1). The size of particles in Figure 1(a and b) are about 60 nm and 17 nm, respectively. The serious aggregation is distinctly shown in Figure 1(a) for particles synthesized by the traditional once-crosslinking method, while a well dispersion of the nanoparticles with the core–shell structure could be found, implying that the novel double-crosslinking method will be helpful for the development of magnetic materials with core–shell structure (Fig. 1(b)). For comparison, the TEM image of the as prepared pure Fe_3O_4 particle was given in Figure 1(c).

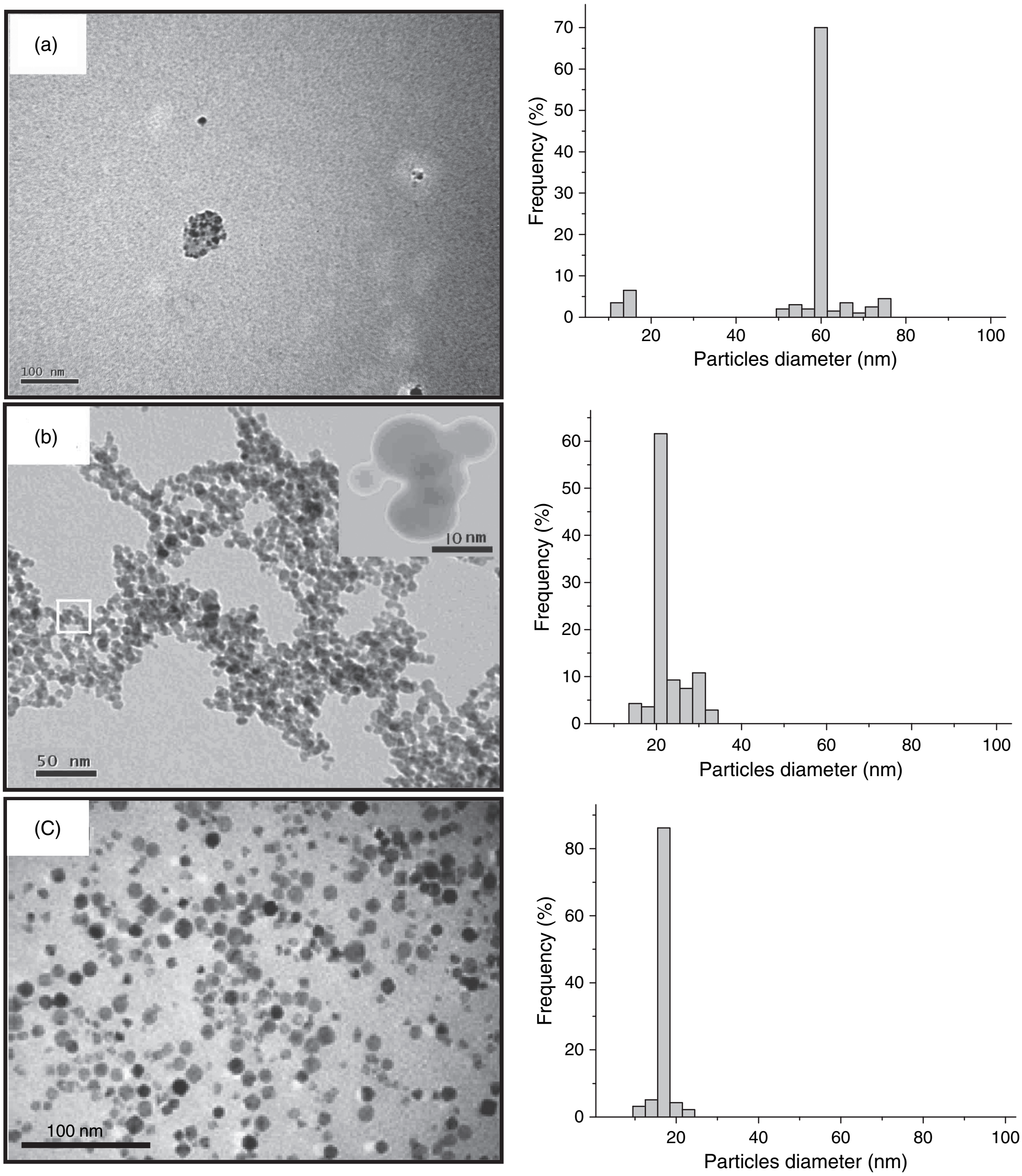

Fig. 1. Representative TEM images for of Fe_3O_4: (a) Fe_3O_4@CS crosslinked once by the traditional method; (b) Fe_3O_4@CS crosslinked twice by novel double-crosslinking method, the insert is the magnefied picture of the area in white square. For comparison, the as prepared Fe_3O_4 nanoparticles were given in (c). The average diameters of the nanoparticles were obtained by measuring about 100 clusters for each sample.

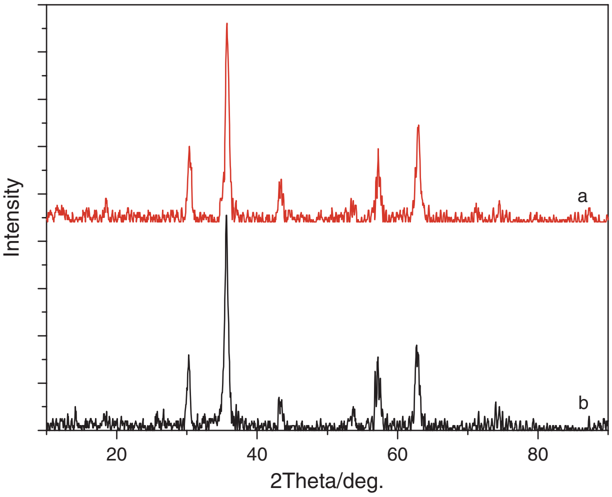

Fig. 2. XRD patterns: (a) for Fe_3O_4 and (b) for Fe_3O_4@CS particles.

3.2. XRD Results

Magnetite (Fe_3O_4) has an inverse spinel structure where O^{2-} ions are cubic close packed (ccp), the Fe^{2+} ions are in octahedral sites, and the Fe^{3+} ions are half in octahedral and half in tetrahedral sites.[27] The typical XRD pattern for as-synthesized pure Fe_3O_4 and Fe_3O_4@CS particles is given in Figure 2. The grain size can be estimated by means of the Debye-Scherrer formula based on the full width at half-maximum (FWHM) of main diffraction peak: $D = K\lambda/FW(S)\cdot\cos\theta$, where D/nm is the crystal size, K is a constant (usually $K = 1$), λ/nm is wavelength of the X ray, FW(S) is the full width at half-maximum of diffraction peaks, and θ is the diffraction angle.[28]

All the diffraction peaks in Figure 2(a), for as synthesized pure Fe_3O_4 can be indexed as the inverse spinel structure magnetite (JCPDS file number 65-3107). The phenomenon of peak broadening displayed indicates that the Fe_3O_4 nanocrystals have a very small grain size (being accurately 11.5 nm by means of Debye-Scherrer formula). The Fe_3O_4@CS particles obtained through the novel double-crosslinking method was also characterized by XRD (see Fig. 2(b)). Since CS is an amorphous material, there is nearly no obvious difference between the XRD patterns of Fe_3O_4 and that of Fe_3O_4@CS, which means that the coating of CS layer would not affect the crystalline structure of Fe_3O_4.

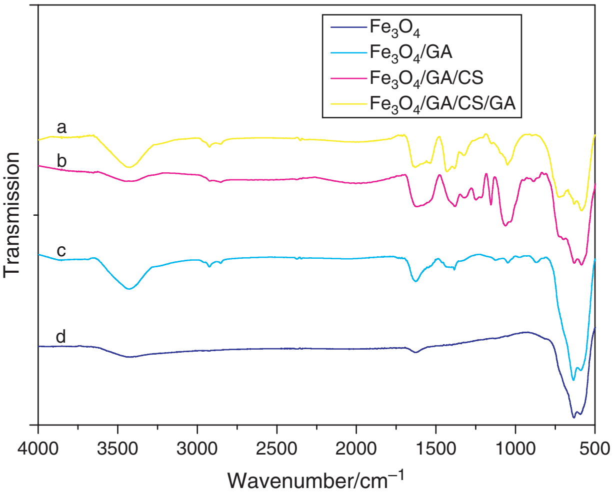

Fig. 3. IR spectra of Fe_3O_4, Fe_3O_4/GA, Fe_3O_4/GA/CS and Fe_3O_4/GA/CS/GA.

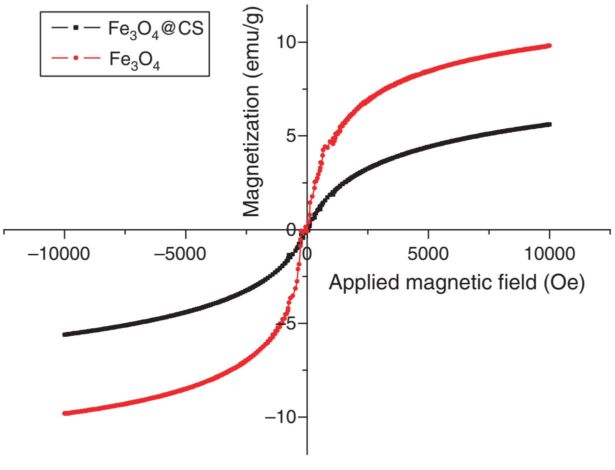

Fig. 4. Field dependence of magnetization for the Fe_3O_4 and Fe_3O_4@CS nanoparticles.

3.3. FTIR Results

To confirm the forming of Fe_3O_4@CS core–shell structure generated from the double crosslinking reaction, FTIR measurements of the Fe_3O_4, Fe_3O_4 adsorbing GA (noted as Fe_3O_4/GA) and Fe_3O_4@CS particles crosslinked before and after loading (noted as Fe_3O_4/GA/CS and Fe_3O_4/GA/CS/GA, respectively) were carried out. The FTIR spectra of different samples are presented in Figure 3. The characteristic absorption bands of pure Fe_3O_4 mainly include those at 570 and 375 cm^{-1}, which

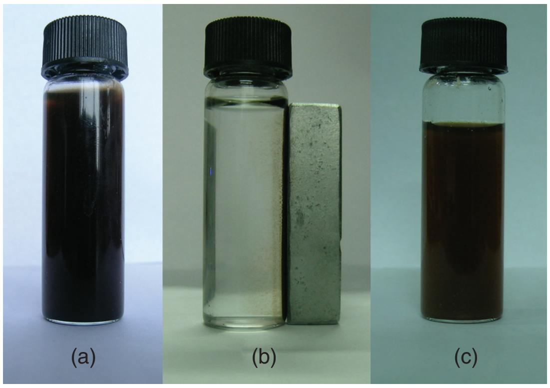

Fig. 5. Optical photograph of the as-obtained Fe_3O_4@CS nanoparticles dispersed in a glass battle: (a) without magnetic field, (b) with magnetic field, (c) after the applied magnetic field was removed.

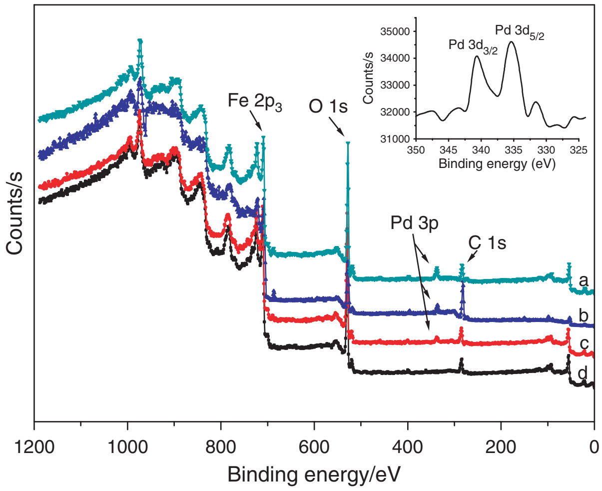

Fig. 6. XPS spectra of samples, (c), (b) and (a) curves for samples refluxed once, two and three times, respectively; (d) curve for the Fe_3O_4@CS without Pd deposition (The insert for Pd 3d).

attributed to Fe–O band. For the as-synthesized Fe_3O_4 particles, the two bands at 634 and 394 cm^{-1} are the consequence of the split of the characteristic absorption of Fe_3O_4 at 570 cm^{-1} that shifts to a higher wavenumber. Similarly, the band at 446 cm^{-1} comes from another absorption band of the Fe–O bond at 375 cm^{-1} of bulk Fe_3O_4. It should be noted that so far the reason behinds the shift of the absorption band of Fe–O bonds of nanoparticles to higher wavenumber is unclear.[29]

With the followed crosslinking process, the IR spectra in Figure 3 show three sets of significant changes (i) The new peaks appearing in curve (c) at 1415, 1720, 2768 and 2854 cm^{-1} (attributed to stretching of C–H of $–CH_3$, C=O, C–H of –CHO and C–H of $–CH_2$, respectively) arising from bonds in GA, which approved the adsorption of GA onto the surface of Fe_3O_4 particles by electrostatic force.[30] (ii) From curve (b) of Fe_3O_4/GA/CS, by use of a combination of the O–H stretching band at 3442 cm^{-1}, amide I bands at 1618 cm^{-1}, amide II band at 1527 cm^{-1}, the bridge oxygen stretching band at 1153 cm^{-1}, and the C–O stretching bands at 1062 and 1035 cm^{-1}, the percent deacetylation can be determined.[31] The peak at 1655 cm^{-1} can be attributed to an imine bond (N=C) and that at 1562 cm^{-1} is associated with an ethylenic bond (C–C), which can be attributed to the increase of the contribution of the glutaraldehyde molecule in the chitosan–glutaraldehyde reaction to cause an increase in the crosslinking chain.[32] (iii) When the second crosslinking was done, the outer CS shell was crosslinked ulteriorly, thus spectra (a) and (b) are very similar besides a small increase in intensity of N=C bond at 1562 cm^{-1}, which shows that the second crosslinking had successfully treated the un-crosslinked CS at the foregone step.

3.4. Analysis of Magnetic Properties

The as-obtained Fe_3O_4@CS nanoparticles are superparamagnetic, which can be proved by the zero coercivity and remanence on a hysteresis loop observed in the magnetization curves recorded at room temperature (shown in Fig. 4). The saturation magnetization (Ms) of buck magnetite is 87 emu/g.[33, 34] However as the particle size decreased to the nanometer scale, the value of Ms will remarkably reduce (here the Ms of Fe_3O_4 is only 9.8 emu/g), which is due to the particle size effects. Meanwhile, the magnetization should be normalized by thermogravimetirc analysis with respect to mass in the Fe_3O_4 sample, considering the fact that the magnetic hybrid nanoparticles have far less content of magnetic substance per gram than iron oxides. The normalized result shows the saturation magnetization of the CS coated sample (~58 emu/g), comparable to results obtained by others for iron oxide nanoparticles.[35] In this case, a dead magnetic layer, mainly made of double-crosslinked CS, is formed over the surface layer due to the strong interaction between the magnetite surface and the CS with the help of the crosslinking agent GA, which prevents the coupled dipoles of Fe_3O_4 particles from aligning along the magnetic orientation. Thus there is a tendency toward lower magnetization values.[36]

The dispersion and magnetic responsive properties of as-obtained Fe_3O_4@CS were vividly given in the optical photographs in Figure 5. Here, Fe_3O_4@CS nanoparticles has a high solubility and dispersibility in water (see Fig. 5(a)) and will not aggregate or precipitate for at least one month, which is highly satisfactory for the practical application. When subjected to a strong magnetic field, the particles can be completely separated from the solution within seconds (see Fig. 5(b)). If the magnetic field is removed and the resulted was vortexed again, the Fe_3O_4@CS particles will re-disperse back into the original solution to form a uniformly dispersed system (see Fig. 5(c)).

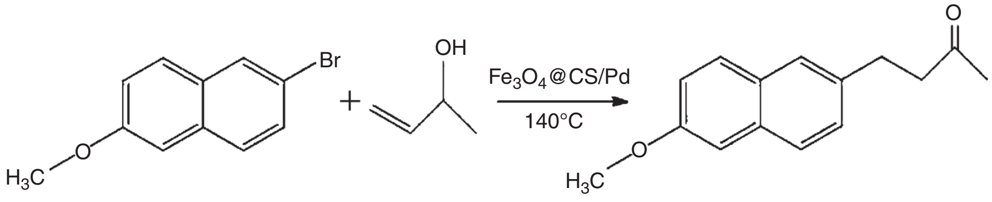

Scheme 2. Schematic drawing of the synthesis of nabumetone.

3.5. Deposition of Palladium and Evaluation of Catalytic Properties

Chitosan is a special kind of national polymer, having amino group on C_2 and hydroxyl group on C_3, which are all equatorial bonds in terms of conformation. This special structure endows this material with a perfect chelating property with some heavy metal ions of appropriate ionic radius, which makes it a hot spot in the field of polymer-metal catalyst.

The treatment of mixing and stirring was to accelerate the rate of Pd^{2+} sorption on chitosan out of chelating function, and the modeling of this sorption isotherm and kinetics was reported by Guibal.[37] By *in-situ* reduction reaction, the reflux treatment transformed the absorbed Pd^{2+} ion to Pd^0 deposition. In order to understand the surface variation of catalyst with the increase in the times of reduction, XPS characterization was employed. Figure 6 shows the full XPS patterns, in which curves (c), (b) and (a) represent catalyst Fe_3O_4@CS/Pd after the first, second and third reduction, respectively. As the reference, curve (d) represent Fe_3O_4@CS without palladium deposition. And the insert in Figure 6 shows XPS patterns of Pd 3d of composite catalyst Fe_3O_4@CS/Pd. For catalyst with different reduction times, the peak of Pd 3d at 336 eV (335 and 340 eV due to Pd $3d_{5/2}$ and Pd $3d_{3/2}$, respectively, in the insert) increased with the reduction times. These results indicate that after the first reduction, Pd atoms were bound to the surface of Fe_3O_4@CS nanoparticles through the coordination of $-NH_2$ ligand with Pd and then grown into bigger clusters when the reduction was performed further, for the later Pd crystallization was initiated by the former Pd as crystal nucleus. The conclusion was also approved by the increase in absorption peaks of UV-Vis for samples after different reduction times (see the SI-1 in the supporting Information part).

Herein, the catalytic activity of Fe_3O_4@CS/Pd was investigated by the experiment of synthesizing nabumetone (one modification of the Heck reactions, the detail could be found in Scheme 2). The product was approved to be nabumetone by IR characterization (see SI-2 in the supporting Information part). The yield was derived from the UV-Vis measurement, and the variation of production yield with the recycle times indicated that the activity decreased slightly from 94.7% at the first time to 89.6% after 20 times (Fig. 7), which suggested that the obtained catalyst had a perfect recycle property. All these results imply the high potential of this resultant to be applied in the filed of magnetic separation.

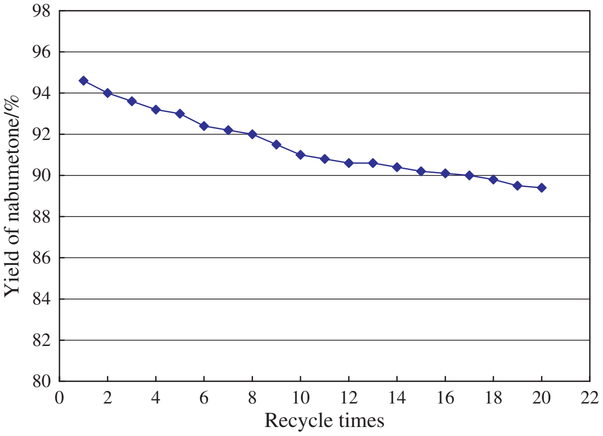

Fig. 7. The relation between yields of nabumetone and cycle index of catalyst.

4. CONCLUSION

In summary, a novel double-crosslinking strategy was put forward to prepare Fe_3O_4@CS hybrid nanoparticles with excellent core/shell structure, and magnetic responsive properties. These superparamagnetic Fe_3O_4@CS nanomaterials are water soluble because of their surface CS layer, so the nanoparticles are easily dispersed in water and thus easily combined to a variety of biological macromolecules, such as peptides, proteins, and nucleic acids. The simple dispersion–separation and re-dispersion experiment results revealed that the as-obtained CS-coated magnetic nanocrystals synthesized by this novel double-crosslinking method possess very good magnetism and water solubility. The deposition of palladium and subsequent synthesis of nabumetone indicated that the obtained Fe_3O_4@CS nanomaterials would function well as one carrier of recycle catalyst.

Acknowledgments: This work was supported by Henan Innovation Project for University Prominent Research Talents (HAIPURT) program, the President Fund of GUCAS, and the KF2008-04, from the State Key Laboratory of Environmental Chemistry and Ecotoxicology, Research Center for Eco-Environmental Sciences, Chinese Academy of Sciences.

References and Notes

1. J. Schoonman, *Solid State Ionics* 135, 5 **(2000)**.
2. V. S. Kalambur, E. K. Longmire, and J. C. Bischof, *Langmuir* 23, 12329 **(2007)**.
3. E. Alsberg, E. Feinstein, M. P. Joy, M. Prentiss, and D. E. Ingber, *Tissue Eng.* 12, 324 **(2006)**.
4. H. Y. Tsai, C. F. Hsu, I. W. Chiu, and C. B. Fuh, *Anal. Chem.* 79, 8416 **(2007)**.
5. H. Chen, M. Kaminski, X. Liu, C. Mertz, Y. Xie, M. Torno, and A. Rosengart, *Med. Hypotheses* 68, 1071 **(2007)**.
6. J. P. Fortin, C. Wilhelm, J. Servais, C. Menager, J. C. Bacri, and F. Gazeau, *J. Am. Chem. Soc.* 129, 2628 **(2007)**.
7. J. Rubio-Retama, N. E. Zafeiropoulos, and C. Serafinelli, *Langmuir* 23, 10280 **(2007)**.
8. Y. Jing, L. R. Moore, and P. S. Williams, *Biotechnol. Bioeng.* 96, 1139 **(2007)**.
9. J. P. Jolivet, C. Chaneac, and E. Tronc, *Chem. Commun.* 5, 481 **(2004)**.

10. A. Pineau, N. Kanari, and I. Gaballah, *Thermochim. Acta.* 447, 89 (**2006**).

11. T. Fried, G. Shemer, and G. Markovich, *Adv. Mater.* 13, 1158 (**2001**).

12. A. B. Bourlinos, A. Bakandritsos, and V. Georgakilas, *J. Mater. Sci.* 41, 5250 (**2006**).

13. S. Z. Wang, H. W. Xin, and Y. T. Qian, *Mater. Lett.* 33, 113 (**1997**).

14. D. Vollath, D. V. Szabó, R. D. Taylor, and J. O. Willis, *J. Mater. Res.* 12, 2175 (**1997**).

15. C. Feldmann and H. O. Jungk, *Angew. Chem. Int. Ed.* 40, 359 (**2001**).

16. R. V. R. Kumar, Y. Koltypin, and Y. S. Cohen, *J. Mater. Chem.* 10, 1125 (**2000**).

17. Z. Zhou, J. Wang, X. Liu, and H. Chan, *J. Mater. Chem.* 11, 1704 (**2001**).

18. F. Vereda, J. de Vicente, and R. Hidalgo-Alvarez, *Langmuir* 23, 3581 (**2007**).

19. N. Pinna, *Chem. Mater.* 17, 3044 (**2005**).

20. G. Zhao, *Chem. Mater.* 17, 3154 (**2005**).

21. M. P. Morales, S. V. Verdaguer, and M. Montero, *Chem. Mater.* 11, 3058 (**1999**).

22. C. C. Berry and A. S. G. Curtis, *J. Phys. D: Appl. Phys.* 36, R198 (**2003**).

23. F. Quignard, A. Choplin, and A. Domard, *Langmuir* 16, 9106 (**2000**).

24. P. A. Sandford, Sources, Chemistry, Biochemistry, Physical Properties and Applications, edited by Chitin and Chitosan, Elsevier Applied Science, New York (**1989**).

25. Y. Ding, Y. Hu, and L. Zhang, *Biomacromolecules* 7, 1766 (**2006**).

26. P. W. Voorhees, *Annu. Rev. Mater. Sci.* 22, 197 (**1992**).

27. R. M. Cornell and U. Schwertmann, The Iron Oxides: Structure, Properties, Reactions, Occurrence and Uses, VCH, New York (**1996**).

28. D. R. Askeland and P. P. Phulé, Essentials of Materials Science and Engineering, Thomson Learning, New York (**2004**).

29. (a) J. Zhang, R. S. Srivastava, and R. D. K. Misra, *Langmuir* 23, 6342 (**2007**); (b) M. Yamaura, R. L. Camilo, and L. C. Sampaio *J. Magn. Magn. Mater.* 279, 210 (**2004**).

30. C. K. Yeom and K. H. Lee, *J. Membrane Sci.* 109, 257 (**1996**).

31. S. Yoshihiro, M. Hiroaki, and S. Hiroyuki, *Int. J. Biol. Macromol.* 18, 237 (**1996**).

32. (a) E. R. Blout, M.Fields, and R. Karplus, *J. Am. Chem. Soc.* 70, 194 (**1948**); (b) A. C. Oyrton, Monteiro, Jr. and A. Claudio, *Int. J. Biol. Macromol.* 26, 119 (**1999**).

33. A. E. Berkowitz, J. A. Lahut, and C. E. Vanburen, *IEEE T. Magn.* 16, 184 (**1980**).

34. J. M. D. Coey, A. H. Morrish, and G. A. Sawatzky, *J. Phys. C: Solid State Phys.* 32, 2386 (**1971**).

35. (a) Y. C. Chang and D. H. Cheng, *J. Colloid Interface Sci.* 283, 446 (**2005**); (b) C. Barrera and C. Rinaldi, *J. Mater. Chem.* 19, 6870 (**2009**).

36. R. Kaiser and G. Midkolczy, *J. Appl. Phys.* 41, 1064 (**1970**).

37. M. Ruiz, A. M. Sastre, and E. Guibal *React. Funct. Polym.* 45, 155 (**2000**).

Received: 11 August 2009. Accepted: 19 October 2009.